Few vs many-body physics of an impurity immersed in a superfluid of spin 1/2 attractive fermions: Supplemental information

M. Pierce,[1] X. Leyronas,[2] and F. Chevy[1]

[1] *Laboratoire Kastler Brossel, ENS-Université PSL, CNRS, Sorbonne Université, Collège de France.*
[2] *Laboratoire de physique de l'Ecole normale supérieure, ENS, Université PSL, CNRS, Sorbonne Université, Université Paris-Diderot, Sorbonne Paris Cité, Paris, France.*

THREE-BODY PHASE-DIAGRAM

In this section, we present an analysis of the three-body problem to determine the stability domain of the Efimov trimers with respect to the free-particle problem and atom-dimer continuum. Specifically, the approach is based on a model with a resonance range R_e. As a consequence, the boundaries of the stability diagram are semi-quantitative and should depend on the model one considers, the goal of this section being also pedagogic.

Efimov ground state

The Efimov spectrum can be obtained without further regularization of the three-body problem using a two-channel model described by the hamiltonian [1, 2]

$$\hat{H} = \sum_{\mathbf{k},\sigma} \epsilon_k \hat{a}^\dagger_{\mathbf{k},\sigma}\hat{a}_{\mathbf{k},\sigma} + \sum_{\mathbf{K},\sigma}(E_{\sigma,0}+\epsilon_k/2)\hat{b}^\dagger_{\mathbf{K},\sigma}\hat{b}_{\mathbf{K},\sigma} + \frac{\hbar^2}{2m}\sqrt{\frac{2\pi}{R_e}}\sum_{\substack{\mathbf{K},\mathbf{k},k<\Lambda \\ \sigma_1\neq\sigma_2\neq\sigma_3}} (\hat{b}^\dagger_{\mathbf{K},\sigma_1}\hat{a}_{\mathbf{k}+\mathbf{K}/2\sigma_2}\hat{a}_{-\mathbf{k}+\mathbf{K}/2,\sigma_3} + \text{H.c.}). \tag{S1}$$

In this expression, $\sigma \in \{1,2,3\}$ labels the three atomic species, $\hat{a}_{\boldsymbol{k},\sigma}$ is the atomic (open channel) annihilation operator for species σ, $\hat{b}_{\boldsymbol{K},\sigma}$ the molecular (closed channel) annihilation operator describing dimers not involving spin σ atoms, and R_e the effective range of the potential. For the sake of simplicity, we assume that all three atomic species have the same mass m and that the atom-dimer coupling is the same for all three species. The atom-atom scattering lengths are nevertheless controlled independently by the bare molecular binding energies $E_{\sigma,0}$.

The solutions of the two-body problem shows that the scattering length a_σ between two atoms $(\sigma_1,\sigma_2) \neq \sigma$ is given by

$$\frac{1}{a_\sigma} = \frac{2}{\pi}\Lambda - \frac{R_e m E_{\sigma,0}}{\hbar^2}, \tag{S2}$$

where Λ is a UV momentum cut-off.

The three-body bound states are described by the Ansatz

$$|\psi\rangle = \sum_{\boldsymbol{k}_1,\boldsymbol{k}_2}\beta(\boldsymbol{k}_1,\boldsymbol{k}_2)\hat{a}^\dagger_{\boldsymbol{k}_1,1}\hat{a}^\dagger_{\boldsymbol{k}_2,2}\hat{a}^\dagger_{-\boldsymbol{k}_1-\boldsymbol{k}_2,3}|0\rangle + \sum_{\sigma,\boldsymbol{k}}\frac{\alpha_\sigma(\boldsymbol{k})}{k}\hat{a}^\dagger_{-\boldsymbol{k},\sigma}\hat{b}^\dagger_{\boldsymbol{k},\sigma}|0\rangle. \tag{S3}$$

where $|0\rangle$ is the vacuum.

The trimer energy $E_3 = -\hbar^2\kappa^2/m$ is then obtained by solving the set of three equations

$$\left[\sqrt{1+3p^2/4} + \kappa R_e(1+3p^2/4) - \frac{1}{\kappa a_\sigma}\right]\alpha_\sigma(p) = \frac{1}{\pi}\int_0^\infty dq \ln\left(\frac{p^2+q^2+pq+1}{p^2+q^2-pq+1}\right)\left[\sum_{\sigma'\neq\sigma}\alpha_{\sigma'}(q)\right], \tag{S4}$$

Frontiers of the stability diagram

We explain here how the different domains of the stability diagram of Fig. S1 are obtained.

In experiments, R_e is small compared to the interparticle distance, therefore we have $R_e\, k_F \ll 1$, where the Fermi wavevector k_F is defined by $n \equiv k_F^3/(3\pi^2)$. On the BCS side of the BEC-BCS crossover of the superfluid, we have $1/(k_F a) < 0$ and $1/|k_F a| \sim 1$ and therefore $|R_e/a| = R_e\, k_F/|k_F a| \ll 1$. For the same reason, the BEC side corresponds to $1/(k_F a) \sim 1$ and we have $R_e/a = R_e\, k_F/(k_F a) \ll 1$. On the graph of Fig. S1, the crossover region of the superfluid is therefore concentrated in a narrow region around the y-axis. The consequence of this separation of scales is that, except in this narrow region, for $R_e/a > 0$, the superfluid is made of weakly interacting tightly bound dimers, while for $R_e/a < 0$, it is made of extremely loose Cooper pairs corresponding essentially to non-interacting fermions (except for superfluid properties).

Concerning the impurity-fermion interaction regime, we have similarly $(k_F a') = (R_e/a')^{-1}(k_F\, R_e)$, which is a small dimensionless number for R_e/a' not too small. Therefore, except in a narrow region around the x-axis in Fig. S1, we have $k_F|a'| \ll 1$.

In the ($R_e/a' < 0$, $R_e/a < 0$) quadrant (Fermi polaron sector), the energy of the impurity immersed in the superfluid is given by $E_{SF} + g'\, n$, where E_{SF} is the ground state energy of the superfluid without the impurity.

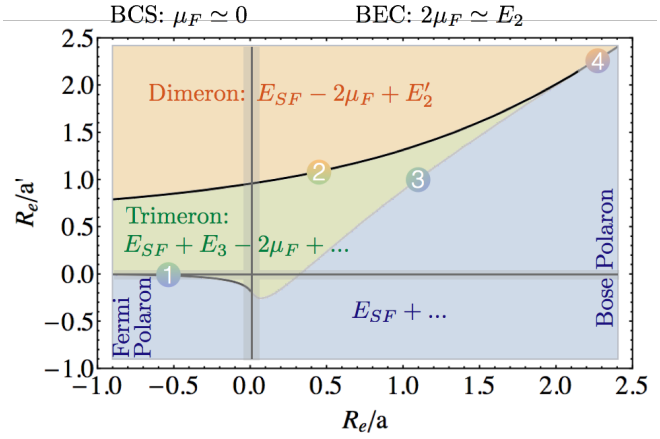

FIG. S1. Phase diagram of an impurity immersed in a fermionic superfluid. The typical energy of each phase (detailed in the text) is written in each domain, the dots in each expression contain the mean-field terms that are negligible compared to the other terms. The typical expression of the chemical potential in the BEC-BCS crossover is given at the top (on the BCS side, it corresponds approximately to the Fermi energy which is negligible compared to the other energy scales presented here, hence the 0). The four numbers correspond to the four frontiers described in the text. The grey bands correspond to the parameter range where many-body effects affect few-body physics for a typical value $k_F R_e = 5 \times 10^{-2}$.

In the Bose-polaron sector ($R_e/a' < 0$, $R_e/a > 0$), the energy of the polaron in the superfluid is given by $E_{SF} + g'_{b-f}\, n$, where g'_{b-f} is the coupling constant between the impurity and a dimer of the superfluid.

In the ($R_e/a' > 0$, $R_e/a < 0$) quadrant the energy of the dimeron in the superfluid is $E_{SF} - 2\mu_f + E_2' + g'_{b-f} n + gn$. The $-2\mu_f$ contribution originates from Cooper pair breaking. One of the fermions of the pair binds to the impurity to form a dimer of energy E_2' while the second remains unbound and contributes to the mean-field term gn. For $R_e/a < 0$, $\mu_f \approx \hbar^2 k_F^2/(2m)$ is the chemical potential of an ideal gas. The dimer energy is given by [3] $E_2' = -\frac{\hbar^2}{m}\kappa_2'^2$, with $R_e\, \kappa_2' = 2\frac{R_e}{a'}\left(1 + \sqrt{1 + 4\frac{R_e}{a'}}\right)^{-1}$.

For ($R_e/a' > 0$), and ($R_e/a > 0$) , the energy of the dimeron in the superfluid is $E_{SF} - E_2 + E_2' + g'_{b-b} n + gn$ where we have substracted the dimer energy E_2 lost by the binding of a fermion of the bath with the impurity. The expression for E_2 is obtained from the expression of E_2' by replacing a' by a. g'_{b-b} is the coupling constant characterizing the interaction between the dimeron and the dimers of the superfluid.

Finally, the energy of the trimeron in the superfluid is given by $E_{SF} + E_3 - 2\mu_f + g'_{t-f} n$. E_3 is the trimer energy (a 3-body bound state), g_{t-f} is a trimer-fermion coupling constant, and $-2\mu_f$ is the energy of the two fermions of the trimer coming from the superfluid bath.

Depending on the parameters, we determine which state has the lowest energy. In this limit where k_F tends to zero, all the terms containing n or k_F vanish. All these energies, minus the neglected mean-field terms, are gathered in Fig. S1. We then consider four cases (corresponding to the four numbers displayed in Fig. S1):

1. Fermi polaron ($R_e/a < 0$) vs trimeron. The frontier is obtained by solving $E_3(R_e, a, a') = 0$.

2. Dimeron vs trimeron. The frontier is obtained by solving $E_3(R_e, a, a') = E_2'$.

3. Bose polaron ($R_e/a > 0$) vs trimeron. The frontier is obtained by solving $E_3(R_e, a, a') = E_2$.

4. Bose polaron vs dimeron. The frontier is obtained by solving $E_2' = E_2$. Since E_2' and E_2 are given by the same function evaluated for a' and a, this frontier is included in the line $a' = a$, *i.e.* the first bisector in S1.

We end this section by noticing that the Fermi polaron-trimeron frontier approaches the x-axis for $Re/a \to -\infty$. In this region, the calculation is no more controlled (k_F is not negligible anymore). However, since the polaron/trimeron is a crossover [4], the transition line cannot be defined precisely anyway.

Moreover we note that for $a = a'$, our results agree with the calculations reported in [3] for three-component color Fermi gases.

BCS THEORY

This section presents a derivation of the results presented in the paper within the simplified framework of BCS mean-field theory. We first determine χ, then the F function and finally we compare it to the exact expressions presented in this paper.

Since these results will only confirm the general behaviour but will not yield quantitative predictions, we restrain our calculations to the simplest case $m_f = m_i = m$ so for $\eta = 1$, a ratio close to the mass ratio we have with our Lithium experiment (7/6).

Mean-field compressibility

As described in the main text, second order perturbation theory relates the polaron energy shift to the fermionic superfluid dynamical compressibility $\chi(\boldsymbol{q}, E)$ defined by

$$\chi(\boldsymbol{q}, E) = \frac{1}{N}\sum_{\alpha} \frac{|\langle\alpha|\hat{\rho}_{-\boldsymbol{q}}|0\rangle|^2}{E_\alpha - E_0 + E}. \tag{S5}$$

Here, we derive the expression of χ using BCS theory where the fermionic medium is described by the mean-field Hamiltonian

$$\hat{H}_{\rm mb} = \sum_{\boldsymbol{k},\sigma} \xi_k \hat{c}^\dagger_{\boldsymbol{k}\sigma}\hat{c}_{\boldsymbol{k}\sigma} + \Delta^* \sum_{\boldsymbol{k}} \hat{c}_{\boldsymbol{k}\uparrow}\hat{c}_{-\boldsymbol{k}\downarrow} + \text{h.c.} \tag{S6}$$

with $\xi_k = \epsilon_k^{(\rm f)} - \mu$, μ is the chemical potential, and the gap Δ is defined by

$$\Delta = \frac{g_0}{\Omega}\sum_{\boldsymbol{k}} \langle \hat{c}_{-\boldsymbol{k}\downarrow}\hat{c}_{\boldsymbol{k}\uparrow}\rangle. \tag{S7}$$

The Hamiltonian is diagonalized by introducing Bogoliubov operators $\hat{\gamma}_{\boldsymbol{k}\pm}$ defined by:

$$\hat{c}_{\boldsymbol{k}\uparrow} = u_k \hat{\gamma}_{\boldsymbol{k}+} - v_k \hat{\gamma}_{-\boldsymbol{k}-} \tag{S8}$$
$$\hat{c}_{\boldsymbol{k}\downarrow} = u_k \hat{\gamma}_{\boldsymbol{k}-} + v_k \hat{\gamma}_{-\boldsymbol{k}+}, \tag{S9}$$

with

$$u_k = \sqrt{\frac{1}{2}(1+\frac{\xi_k}{E_k})}, \quad v_k = \sqrt{\frac{1}{2}(1-\frac{\xi_k}{E_k})} \tag{S10}$$

and $E_k = \sqrt{\xi_k^2 + |\Delta|^2}$.

To derive the BCS expression of the compressibility, we express the matrix elements $\langle\alpha|\hat{\rho}_{-\boldsymbol{q}}|0\rangle = \sum_\sigma \langle\alpha|\hat{c}^\dagger_{\boldsymbol{k}-\boldsymbol{q},\sigma}\hat{c}_{\boldsymbol{k},\sigma}|0\rangle$ using the Bogoliubov creation and annihilation operators. After a straightforward calculation, we finally obtain

$$\chi^{\rm MF}(\boldsymbol{q}, E) = \frac{1}{N}\sum_{\boldsymbol{k}} \frac{2u_{k-q}^2 v_k^2 + 2u_k v_k u_{k-q} v_{k-q}}{E_k + E_{k-q} + E}, \tag{S11}$$

where we have used the fact that the excited states $|\alpha\rangle$ correspond to pairs of Bogoliubov excitations, hence $E_\alpha - E_0 = E_k + E_{k-q}$. We use the notation MF to signify that this result is only valid in BCS theory, a mean-field theory.

Perturbative calculation of the energy

In order to calculate the polaron energy shift, we need to consider the perturbative development we obtained in the article, adapted to BCS theory:

$$\Delta E^{\rm MF}_{\rm pert} = \left[g'n + \frac{g'^2 n}{\Omega}\sum_{\boldsymbol{q}} \left(\frac{1}{\varepsilon_q^{(\rm r)}} - \chi^{\rm MF}(\boldsymbol{q}, \varepsilon_q^{(\rm i)}) \right) \right] \tag{S12}$$

After turning sums to integrals and performing the angular integrations we can write this expression as:

$$\Delta E^{\rm MF}_{\rm pert} = g'n + \frac{g'^2}{8\pi^4}\frac{m}{\hbar^2}\int k^2 \mathrm{d}k \int q^2 \mathrm{d}q \left(\frac{4v_k^2}{q^2} - \frac{2u_q^2 {v_k}^2 + 2u_k v_k u_q v_q}{kq} \ln\left(\frac{E_k + E_q + \frac{\hbar^2(k+q)^2}{2m}}{E_k + E_q + \frac{\hbar^2(k-q)^2}{2m}} \right) \right) \tag{S13}$$

To study the behaviour of these integrals for high k, we perform the variable change $k \to u = (k/k_F)/\sqrt{|\Delta|/E_F}$, $q \to v = (q/k_F)/\sqrt{|\Delta|/E_F}$ and we get

$$\Delta E^{\rm MF}_{\rm pert} = g'n \left[1 + k_F a' \frac{3}{2\pi} \left| \frac{\Delta}{E_F} \right|^2 I(\Lambda/k_F) \right] \tag{S14}$$

with I corresponding to the integral left to calculate in Eq. (S13) that depends on the cut-off Λ and also on the ratio $\mu/|\Delta|$.

In the limit $u, v \gg 1$, we can simplify greatly the expression of the integral I.

First, we can see that the terms u_k^2 and v_k^2 can be rewritten, in this limit:

$$u_k^2 \sim 1, \quad v_k^2 \sim \frac{1}{4}\frac{|\Delta|^2}{\xi_k^2} \to \frac{1}{4u^4} \tag{S15}$$

From this last expression, we can also get Tan's contact for two fermions C_2 in BCS theory. Indeed, using the property of momentum distribution [5]:

$$n_\uparrow(k) \underset{k\to\infty}{\sim} n_\downarrow(k) \underset{k\to\infty}{\sim} \frac{C_2}{k^4} \tag{S16}$$

and knowing that in BCS theory we have $n(k) = n_\uparrow(k) + n_\downarrow(k) = 2v_k^2\Omega$, we see that we have the right dependence for the momentum distribution and we can extract the contact

$$\frac{C_2}{N} = \frac{3\pi^2}{4}\left|\frac{\Delta}{E_F}\right|^2 k_F. \tag{S17}$$

The integral can then be simplified in this limit as

$$I(\Lambda/k_F) = \int \frac{\mathrm{d}u}{u}\int \frac{\mathrm{d}v}{u}\left[1 - \frac{1}{2}\left(\frac{v}{u} + \frac{u}{v}\right)\ln\left(\frac{1 + v/u + (v/u)^2}{1 - v/u + (v/u)^2}\right)\right]. \tag{S18}$$

The second integral (over v/u) converges towards $2\pi^4\kappa^{\rm MF}$ and the first integral (over u) gives the logarithmic divergence. We can finally write:

$$I = 2\pi^4\kappa^{\rm MF}(\ln(\Lambda/k_F) + ...) \tag{S19}$$

with κ^{MF}:

$$\kappa^{\mathrm{MF}} = \frac{\sqrt{3}}{8\pi^3} - \frac{1}{12\pi^2}. \tag{S20}$$

In the main text we found:

$$\kappa(1) = \frac{\sqrt{3}}{8\pi^3} - \frac{1}{12\pi^2} - \frac{1}{9\pi\sqrt{3}} \tag{S21}$$

The two results are very similar except for the last term of $\kappa(1)$ which does not appear in the mean-field approach because BCS theory does not account for interactions between excitations of the superfluid. This missing term is actually pretty important since it is the leading term in κ, therefore we get a ratio $\kappa(1)/\kappa^{\mathrm{MF}} \simeq 15$.

The F function

We find out analytically that there is again a logarithmic divergence of this second order term, consistently with what we stated before. By combining equations (S14), (S17) and (S19), we get the expression of the energy calculated up to second order in perturbation using BCS theory :

$$\Delta E^{\mathrm{MF}}_{\mathrm{pert}} = g'n\left[1 + k_F a' F^{\mathrm{MF}}\left(\frac{1}{k_F a}\right) + 4\pi\kappa^{\mathrm{MF}} a' \frac{C_2}{N}\ln(\Lambda/k_F)\right] \tag{S22}$$

with F^{MF} a function that can be computed numerically throughout the BEC-BCS crossover by calculating the difference between the exact expression of the integral I defined in Eq. (S13) and the logarithmic term we obtained in Eq. (S19). These numerical calculations show that this function does not depend on the cut-off but only on the parameter $1/(k_F a)$.

Then, by introducing a similar renormalization with a three-body term, we can rewrite the energy as:

$$\Delta E^{\mathrm{MF}} = g'n\left[1 + k_F a' F^{\mathrm{MF}}\left(\frac{1}{k_F a}\right) - 4\pi\kappa^{\mathrm{MF}}\frac{a' C_2}{N}\ln(k_F R_3) + ...\right], \tag{S23}$$

We get a very similar expression to the one we found in this letter, only we replaced F and $\kappa(1)$ by F^{MF} and κ^{MF}.

The function F^{MF} is represented in Fig. S2, and we can observe the two asymptotic behaviours on the BCS and BEC sides:

1. In the BCS limit we recover once again the Fermi-polaron, hence $F^{\mathrm{MF}}(-\infty) = 3/2\pi$ for $\eta = 1$.

2. In the BEC limit, we get a behaviour consistent with the Bose-Polaron:

$$F^{\mathrm{MF}}\left(\frac{1}{k_F a}\right) = 16\pi^2\kappa^{\mathrm{MF}}\frac{\ln(k_F a)}{k_F a} + ... \tag{S24}$$

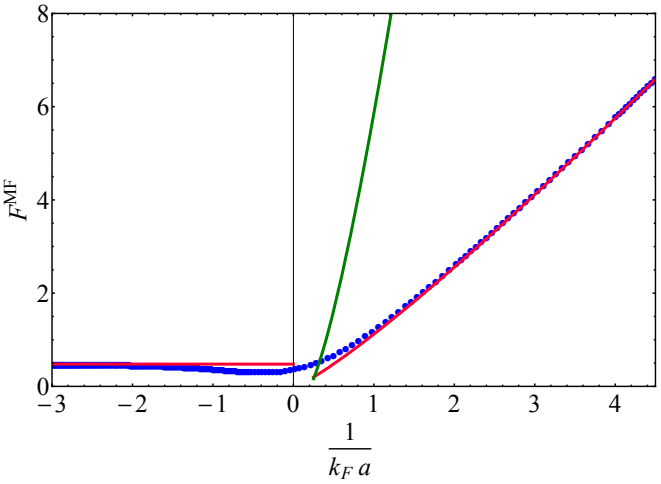

FIG. S2. Blue dots: Representation of the function F^{MF} through the crossover for $\eta = 1$. Red curves: Asymptotic behaviours described in the text on the BCS side: $F^{\mathrm{MF}}(-\infty) = \frac{3}{2\pi}$, and the BEC Side : $F^{\mathrm{MF}}(X) \simeq 16\pi^2\kappa^{\mathrm{MF}} X\ln(1/X) + A_0 X$ with A_0 an adjustable parameter found out to be, after optimization, $A_0 \simeq 1.1$. Green curve: asymptotic behaviour on the BEC side using the true value of κ, C_{ad} and R_3 (the last two are given in the last section of this Supplementary material).

In conclusion, BCS theory predicts the correct qualitative behaviour for the polaron energy shift but is quantitatively wrong, which is illustrated in Fig. S5 at the end of this supplementary material.

THREE-BODY PARAMETERS

Calculating R_3

We can obtain the three-body parameter R_3 introduced in the equation

$$\Gamma_{\mathrm{Born}} - \Gamma_{\mathrm{Faddeev}} \underset{\Lambda\to\infty}{=} g'^2\kappa(\eta)\ln(\Lambda R_3) + o(1) \tag{S25}$$

by calculating numerically this difference. We break down this term into three parts, each corresponding to one of the first three diagram of Fig. 2 from this letter.

Firstly, in the effective range approximation, the two-body T-matrix is given by

$$\hat{t}_i = \frac{g'/\Omega}{1 + ika' + R_e a' k^2} \tag{S26}$$

where R_e is the effective range of the potential and k is given by:

$$k = \sqrt{2m_r(E + i0^+)/\hbar^2} \tag{S27}$$

with E the energy of the initial state in the center-of-mass frame of the three particles at the moment of the interaction. For the diagrams we want to calculate, we only have to consider the case where the fermions have impulsions of $\boldsymbol{p}$ and $-\boldsymbol{p}$ and the impurity has an impulsion equal to zero (cf Fig. 2 from the article). This leads to:

$$E/\hbar^2 = 0 - (\frac{p^2}{2m_f} + \frac{p^2}{2(m_f+m_i)}) = -\sqrt{\frac{\eta(2+\eta)}{(1+\eta)^2}}\frac{p^2}{m_r} \tag{S28}$$

Finally, the two-body T-matrix can be written as:

$$\hat{t}_i = \frac{g'/\Omega}{1 - \sqrt{\frac{\eta(2+\eta)}{(1+\eta)^2}}a'p - \frac{\eta(2+\eta)}{(1+\eta)^2}(\frac{R_e}{a'})(a'p)^2 + i0^+} = \frac{g'}{\Omega}t(p) \tag{S29}$$

Then, we can write below the expressions corresponding to each of these three diagrams.

$$\Gamma^{(1)} = 2\frac{m_f^2}{\hbar^4}\frac{g'}{\Omega}\sum_{\boldsymbol{p}}\frac{1}{p^4}t(p) \tag{S30}$$

$$\Gamma^{(2)} = -2\frac{m_f^3}{\hbar^6}\frac{g'^2}{\Omega^2}\sum_{\boldsymbol{p_1},\boldsymbol{p_2}}\frac{1}{p_1^2p_2^2}\frac{t(p_1)t(p_2)}{(p_1^2+p_2^2)(\frac{\eta+1}{2\eta}) - \frac{1}{\eta}\vec{p_1}.\vec{p_2}} \tag{S31}$$

$$\Gamma^{(3)} = 4\frac{m_f^3}{\hbar^6}\frac{g'^2}{\Omega^3}\sum_{\boldsymbol{p_1},\boldsymbol{p_2},\boldsymbol{p_3}}\left[\frac{1}{p_1^2p_3^2}\frac{4\pi}{1/a - p_2\sqrt{\frac{\eta+2}{4\eta}}}\right. \\ \left.\times\frac{t(p_1)}{p_1^2+p_2^2(\frac{\eta+1}{2\eta}) - \vec{p_1}.\vec{p_2}}\frac{t(p_3)}{p_3^2+p_2^2(\frac{\eta+1}{2\eta}) - \vec{p_3}.\vec{p_2}}\right] \tag{S32}$$

In order to calculate the Faddeev term for Γ, one has to use the expression of $t(p)$ given in S29. On the other hand, to obtain the Born term, one has to expand this expression of $t(p)$ up to first order in a' for $\Gamma^{(1)}$ and up to zero order for the other two components (so just replacing it by 1), so that all three components of Γ are expanded up to order two in a'.

For $\Gamma^{(3)}$, we calculate the sum in the limit $1/a \ll 1/a'$ (highly interacting fermions) in which the difference between the Faddeev term and the Born term does not depend on a. To calculate these different sums we proceed similarly as we did in the previous section for BCS theory.

In this framework, one can show that R_3/a' only depends on the ratio R_e/a' and the mass ratio. We show in Fig. S3 the numerical calculations of the difference $\Gamma_{\text{Born}} - \Gamma_{\text{Faddeev}}$ for the mass ratio $\eta = 7/6$ and $R_e/|a'| = 1$. We see that we indeed get the logarithmic behaviour with $\kappa(7/6)$ as the proportionality constant.

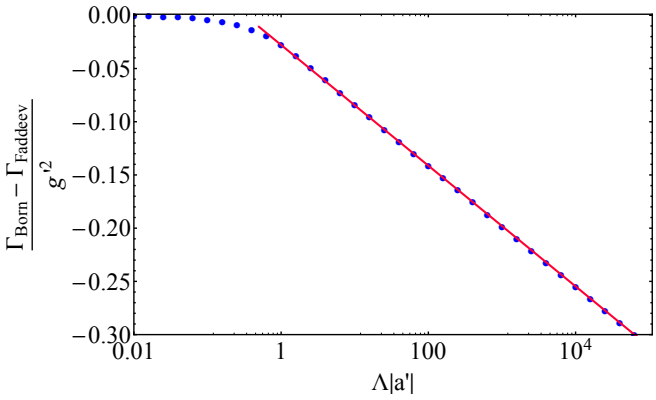

FIG. S3. Blue dots: numerical calculations of the left-hand side of eq. (S25), divided by g'^2, for $\eta = 7/6$ and $R_e = |a'|$. Red curve: fitting curve of the blue dots in the limit $\Lambda|a'| \gg 1$. We fit the data for $\Lambda|a'| \gg 1$ with the function $\kappa(7/6)\ln(X \times A_0)$ with A_0 a fitting parameter. The parameter A_0 gives us the value of $R_3/|a'|$: here we get $A_0 \simeq 3.10$.

We show in Fig. S4 the parameter $R_3/|a'|$ for different values of the ratio $R_e/|a'|$ in the case $\eta = 7/6$. For $R_e/|a'| \ll 1$, we get the asymptotic behaviour $R_3 \simeq 1.50|a'|$. For $R_e/|a'| \gg 1$, we see that R_3 increases exponentially:

$$R_3 \underset{\frac{R_e}{|a'|}\gg 1}{\propto} \sqrt{R_e|a'|}\exp\left(\frac{\sqrt{3}}{16\pi^2|\kappa(7/6)|}\sqrt{\frac{R_e}{|a'|}}\right). \tag{S33}$$

At this point we should remind that we consider expansions for $\Lambda|a'| \ll 1$ but with $R_e/|a'|$ as an independent parameter with a given value. Consequently, we consider this exponential term as a constant included in R_3 in our perturbative calculations.

To see the dependence on the mass ratio η, Table I lists numerical values of the parameter R_3 that were computed for experimentally relevant mass ratios and $R_e = 0$.

η	7/40	23/40	7/6	87/6	133/6
R_3/a'	1.03	1.41	1.50	1.46	1.46

TABLE I. Dimensionless parameter characterizing the Born expansion of the three-body scattering amplitude (Eq. (S25)) for $R_e = 0$.

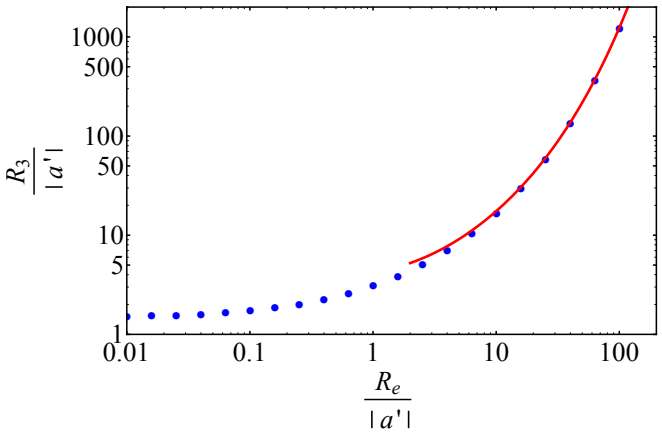

FIG. S4. Blue dots: numerical calculations of $R_3/|a'|$ for different $R_e/|a'|$ ratios and $\eta = 7/6$. Red curve: fit for $R_e/|a'| \gg 1$ using a function $A\sqrt{X}\exp\left(\frac{\sqrt{3}}{16\pi^2|\kappa(7/6)|}\sqrt{X}\right)$, with A an adjustable parameter. $A \simeq 0.8$ after optimization.

Atom-dimer scattering

The atom-dimer T-matrix can be computed using the same approach. Indeed, since the fermions are asymptotically bound, we can treat the impurity-fermion interaction as a perturbation. This leads to the same diagrams as in the three-body scattering problem and the atom-dimer scattering length consequently suffers from the same logarithmic divergence when the range of the potential vanishes. For large Λ the associated T-matrix scales as

$$T_{\rm ad}^{(1)} = \frac{2g'}{\Omega}\left[1 + 8\pi^2\frac{m_f}{m_r}\kappa(\eta)\frac{a'}{a}\left(\ln(\Lambda a) + C_{\rm ad} + ...\right)\right] \tag{S34}$$

where the constant $C_{\rm ad}$ is computed numerically and is given in Table II for experimentally relevant values of the impurity-fermion mass ratios.

η	7/40	23/40	7/6	87/6	133/6
$C_{\rm ad}$	1.52	1.59	1.56	1.37	1.36

TABLE II. Dimensionless parameter characterizing the Born expansion of the atom-dimer scattering amplitude (Eq. (S34)) for $R_e = 0$.

The logarithmic divergence is once again cured by introducing the three-body interaction. Using the renormalized expression of $g_3(\Lambda)$ the three-body interaction contribution to the atom-dimer T-matrix amounts to

$$T_{\rm ad}^{(2)} = -\frac{16\pi^2 g'}{\Omega}\frac{m_f}{m_r}\kappa(\eta)\frac{a'}{a}\ln(\Lambda R_3). \tag{S35}$$

We indeed recover the asymptotic result Eq. [20] from the main text since we have

$$T_{\rm ad} = T_{\rm ad}^{(1)} + T_{\rm ad}^{(2)} = T_{\rm ad,Born}\left[1 - 8\pi^2\frac{m_f}{m_r}\kappa(\eta)\frac{a'}{a}\left(\ln(R_3/a) + C_{\rm ad} + ...\right)\right] \tag{S36}$$

where $T_{\rm ad,Born} = 2g'/\Omega$ corresponds to an atom-dimer scattering length $a_{\rm ad,Born}/a' = 4(1+\eta)/(2+\eta)$. As pointed out in [6], in the Efimovian regime $R_e \ll |a'|$ not considered here, $T_{\rm ad}$ acquires a log-periodic dependence in a'.

Finally, to highlight the shortcomings of BCS theory and the consistency of our three-body calculations, we fit the atom-dimer scattering length calculated in [7], see Fig. S5. There is no hesitation possible in seeing that the coefficient before the log obtained through BCS theory (including $\kappa^{\rm MF}$) is too small to show the logarithmic behaviour whereas the real κ enables a much better fit.

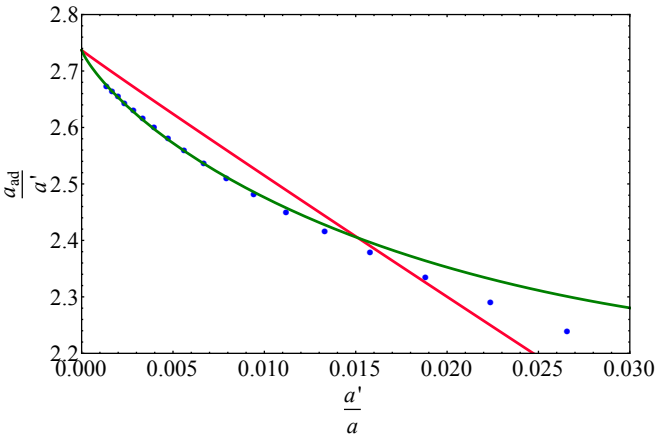

FIG. S5. Blue dots: Points from [7] showing the ratio of the atom-dimer scattering length $a_{\rm ad}$ over a', for $\eta = 7/6$. Red solid curve: fit to the blue dots using the function $a_{\rm ad,\,Born}/a'(1 + AX(\ln X + B))$ where A is a fixed parameter corresponding to the analytical result obtained through BCS theory ($A \propto \kappa^{\rm MF}$) and B is an adjustable parameter. Green solid curve: theoretical curve obtained through three-body calculations, its equation is the same as the one used for the red curve but now with $A \propto \kappa$ and B obtained through $C_{\rm ad}$ and R_3. We see that the curve corresponding to BCS theory (red) does not match at all the results reported in [7], contrary to the other one (green).

[1] Alexander O Gogolin, Christophe Mora, and Reinhold Egger. Analytical solution of the bosonic three-body problem. *Physical Review Letters*, 100(14):140404, 2008.

[2] Mattia Jona-Lasinio and Ludovic Pricoupenko. Three resonant ultracold bosons: Off-resonance effects. *Physical Review Letters*, 104(2):023201, 2010.

[3] Yusuke Nishida. New type of crossover physics in three-component Fermi gases. *Physical Review Letters*, 109(24):240401, 2012.

[4] Yusuke Nishida. Polaronic atom-trimer continuity in three-component Fermi gases. *Physical Review Letters*, 114(11):115302, 2015.

[5] S. Tan. Large momentum part of a strongly correlated Fermi gas. *Ann. Phys.*, 323(12):2971–2986, 2008.

[6] Xiaoling Cui. Atom-dimer scattering and stability of Bose and Fermi mixtures. *Phys. Rev. A*, 90:041603, Oct 2014.

[7] Ren Zhang, Wei Zhang, Hui Zhai, and Peng Zhang. Calibration of the interaction energy between Bose and Fermi superfluids. *Phys. Rev. A*, 90(6):063614, 2014.